THE ASTROPHYSICAL JOURNAL SUPPLEMENT SERIES, 119:59–74, 1998 November

CS EMISSION FROM BOK GLOBULES: SURVEY RESULTS

RALF LAUNHARDT,[1,2] NEAL J. EVANS II,[3] YANGSHENG WANG,[3,4,5] DAN P. CLEMENS,[6]
THOMAS HENNING,[1] AND JOÃO L. YUN[7]

Received 1998 February 3; accepted 1998 June 4

ABSTRACT

We present the results of a survey for CS emission toward a sample of 47 Bok globules selected from the catalog of Clemens & Barvainis. The globules were observed at the FCRAO 14 m, the SEST 15 m, and the IRAM 30 m telescopes in the CS $J = 2 \rightarrow 1$ transition. Additionally, higher spatial resolution (11″–30″) observations in the CS $J = 3 \rightarrow 2$ and $5 \rightarrow 4$ lines, as well as the $C^{34}S$ $J = 2 \rightarrow 1$ and $3 \rightarrow 2$ lines, were carried out toward a subsample of 20 globules using the IRAM 30 m and the CSO 10 m telescopes. Two-thirds of the globules were detected in the CS $J = 2 \rightarrow 1$ line. The detection rate was higher in globules with *IRAS* sources (72%) than in globules without *IRAS* sources (44%). The detection rate was 100% for globules with embedded Class 0 and Class I infrared sources, dropping to 60% for Class II-D sources and to 40% for Class II sources. These results support the association of dense cores with *IRAS* point sources in Bok globules and indicate that the dense gas is most apparent in the early stages. We present CS maps of 12 globule cores and derive sizes for nine CS cores. The results of the CS survey are compared with the results of surveys of other lines and of dust continuum emission. The integrated intensities of the CS lines correlate with those of $C^{18}O$ $J = 2 \rightarrow 1$, but the line widths and FWHM sizes tend to be somewhat larger than those of $C^{18}O$. The mean FWHM size of those sources with reasonable distance estimates is 0.41 ± 0.18 pc, and the mean virial mass is $60 \pm 52\ M_{\odot}$. The mean size places them intermediate between cores in Taurus and cores associated with water masers and massive star formation.

Subject headings: ISM: clouds — ISM: globules — ISM: molecules — radio lines: ISM

1. INTRODUCTION

Bok globules are ideal laboratories for studying star formation in relatively simple environments. A number of earlier studies in molecular lines toward Bok globules have provided information about their structure and their possible connections with star formation (Martin & Barrett 1978; Leung, Kutner, & Mead 1982; Villere & Black 1982). Owing to their relative isolation and simple geometry, Bok globules are also promising sites to search for signatures of gravitational collapse. Zhou et al. (1993, 1994a), for example, found kinematic evidence for collapse in the well-studied globule B335 (see also Chandler & Sargent 1993; Velusamy, Kuiper, & Langer 1995; and Choi et al. 1995), and Wang et al. (1995, hereafter WEZC95) identified several other candidates for collapse in a survey of globules.

Recent discoveries of infrared point sources with *IRAS* and molecular outflows at millimeter wavelengths in many Bok globules have greatly expanded the list of potential protostars and young stars in globules and have provided strong support for the early suggestion that some Bok globules are in the process of forming stars (Bok & Reilly 1947). Clemens & Barvainis (1988, hereafter CB) presented a catalog of 248 optically selected globules; a high percentage (about 44%) had *IRAS* sources within their boundaries. Adopting more stringent criteria and using *IRAS* co-added images, Yun & Clemens (1990, hereafter YC90) found that 23% of the CB globules had evidence for embedded infrared sources. Comparison of the characteristics of the infrared sources associated with globules with those of the field stars indicates that the sources in globules have colors and spectral energy distributions typical of embedded young stellar objects (YSOs) (Yun 1993). Yun & Clemens (1992, hereafter YC92) surveyed 41 of these globules in CO and found that 14 (34% of their sample) have outflows, evidence for ongoing star formation activity. A similar outflow detection rate of 31% was found for a sample of 35 southern globules by Henning & Launhardt (1998).

Despite the strong evidence for star formation in Bok globules and the detailed observations toward one well-studied globule, B335, the connection between the infrared sources detected by *IRAS* and the presence of dense cores is not well established for Bok globules in general. Surveys toward globules using molecular lines that trace dense gas would help to establish such a connection. Recent studies have been carried out in CO and isotopic lines (YC92; Turner 1994a; WEZC95), NH_3 (Kane, Clemens, & Myers 1994; Bourke et al. 1995; Turner 1993; Lemme et al. 1996), HC_3N (Kane et al. 1994), H_2CO (Turner 1994b; WEZC95), and HCN (Afonso, Yun, & Clemens 1998) lines as well as in the radio (Moreira et al. 1997), millimeter (Launhardt & Henning 1997; Henning & Launhardt 1998), and submillimeter (Launhardt, Ward-Thompson, & Henning 1997) continuum.

The present survey focuses on lines of CS and its isotope, $C^{34}S$. The advantage of CS over many other species as a density tracer is that many different rotational lines are easily accessible in the millimeter and submillimeter regime. Detection of CS emission would imply the existence of dense gas in these globules. The isotopic $C^{34}S$ lines are less opaque and provide constraints on the line opacity.

[1] Astrophysical Institute and University Observatory Jena, Schillergässchen 2-3, D-07745 Jena, Germany.
[2] Max-Planck-Institut für Radioastronomie, Bonn, Germany.
[3] Astronomy Department, The University of Texas, Austin, TX 78712.
[4] MRAO, University of Cambridge, Cambridge CB3 0HE, England.
[5] Fidelity Management and Research, Fidelity Investment Systems Co., 400 East Las Colinas Boulevard, CC2E, Irving, TX 75039.
[6] Astronomy Department, Boston University, Boston, MA 02215.
[7] Physics Department, The University of Lisbon, Portugal.

This paper presents a summary of CS observations performed at four different telescopes. The Five College Radio Observatory (FCRAO) 14 m telescope was used to map the CS $J = 2 \rightarrow 1$ emission toward the YSOs that had previously been searched for outflows by YC92; the Institute de Radio Astronomie Millimetrique (IRAM) 30 m telescope was used to obtain higher spatial resolution data in several transitions including the isotopic lines; and the 15 m Swedish-ESO-Submillimeter Telescope (SEST) was used to observe the CS $J = 2 \rightarrow 1$ line toward southern globules, including seven not observed with FCRAO and IRAM. The Caltech Submillimeter Observatory (CSO) 10 m telescope was used to observe CS $J = 5 \rightarrow 4$ emission. These combined data provide information on the incidence and morphology of dense cores in Bok globules.

In § 2, we describe the sample selection and the observations. The results are presented in §3, while the discussion may be found in § 4.

2. SAMPLE SELECTION AND OBSERVATIONS

2.1. *Sample Selection*

The globules studied in this paper are selected from the catalog of CB. The major focus of the CS line survey presented here was to investigate the properties of star-forming cores in Bok globules. Therefore, the selection criteria were adjusted to include globules with evidence of ongoing star formation.

Thirty-eight globules that have *IRAS* point sources within their optical boundaries ("core-type" *IRAS* sources; see CB) were selected, of which 30 sources were detected in all four wavelengths by Clemens, Yun, & Heyer (1991) in their analysis of the *IRAS* co-added images. Thirty-one of the selected globules were also observed in the 1.3 mm continuum by Launhardt & Henning (1997, hereafter LH97). All CO outflow sources (12) found by YC92 and all sources detected in the 1.3 mm continuum (17) by LH97 were included in the sample. Twenty-seven of these 38 globules were also observed in the $C^{18}O$ $J = 2 \rightarrow 1$ line by WEZC95.

We have classified the globules with *IRAS* point sources according to their infrared spectral energy distributions (SED). The characteristics of the source's SED are given in terms of the class system (see Lada 1987), originally running from I to III, with Class I the youngest and most embedded. Class II-D resembles the near-infrared properties of Class II but has a strong far-infrared excess (see Wilking, Lada, & Young 1989). Recently the system has been extended to still younger, more embedded objects, referred to as Class 0 objects (André, Ward-Thompson, & Barsony 1993).

Our sample of 38 target objects (globules with *IRAS* sources) includes four Class 0 candidates, 13 Class I sources, five Class II-D sources, and nine Class II sources. The sample includes eight other *IRAS* point sources without sufficient information to be classified. Caution is required when interpreting this classification in terms of evolutionary stages of the individual objects. None of the Class 0 candidates has yet been shown to fulfill all the criteria used to define Class 0. There may also be confusion between Classes I and II-D owing to projection effects in aspherical geometries. Some sources were found to be multiple at near-infrared wavelengths (e.g., CB 34, Alves & Yun 1995; CB 205, Neckel & Staude 1990), so that only "effective" SEDs were measured by *IRAS*. A more detailed discussion of the evolutionary stage of a subsample of globule cores will be undertaken on the basis of spatially resolved photometric infrared and millimeter continuum data (Launhardt, Zylka, & Henning 1998b).

Table 1 lists names, coordinates, the radial velocities used for the observations ($V_{\rm LSR}$), and the classification of the 38 globules associated with *IRAS* point sources. Two *IRAS* point sources were observed in CB 58. All but two source positions are from the *IRAS* Point Source Catalog (IPSC); the other two positions are from YC92 (CB 12) and from CB (CB 82). The main sample is obviously biased toward globules that might be forming stars and therefore is not representative of Bok globules in general.

To correct for this bias, a control sample of nine globules showing no spatial correlation with any *IRAS* point sources ("starless" globules; Table 2) was added, so that the total number of globules observed amounts to 47. Three of these "starless" globules, CB 44, CB 231, and CB 233, were studied by Leung et al. (1982) in CO. Two other globules, CB 98 and CB 246, were detected in the 1.3 mm continuum by LH97. The remaining sources were taken from YC92.

2.2. *Observations*

Observations were carried out at four different telescopes: the 14 m telescope of the FCRAO, the IRAM 30 m telescope, the 15 m SEST, and the 10 m CSO. Table 3 summarizes the characteristics of the four telescopes. The main beam efficiencies ($\eta_{\rm mb} = B_{\rm eff}/F_{\rm eff}$) are typically uncertain by about 10% of the values in the table. For the IRAM efficiencies, an uncertainty of $\pm 15\%$ has been assigned since antenna surface adjustments and systematic efficiency measurements with all receivers were performed after our observations.

The standard chopper wheel calibration procedure (Penzias & Burrus 1973; Kutner & Ulich 1981) was used at all four telescopes. The resulting antenna temperature, T_A^*, is corrected for atmospheric attenuation and all telescope losses. Division of T_A^* by $\eta_{\rm mb}$, the telescope main-beam efficiency, yields the main-beam radiation temperature, $T_{\rm mb}$. Details of the observations are described in the following sections. The observing parameters are summarized in Table 3.

2.2.1. *FCRAO Observations*

Thirty globules (see Table 4) were mapped in the CS $J = 2 \rightarrow 1$ line using the FCRAO 14 m telescope during two runs in 1993 March and May. The 15 beam receiver array, QUARRY (Erickson et al. 1992), was used to map the globules. For most of the sources, we mapped at full-beam spacings covering an area of about $4' \times 5'$. Maps with Nyquist sampling covering the same area were also made toward a few sources. The map centers were taken from YC92 for sources surveyed for CO outflows and from CB for "starless" globules. The backend spectrometer was a 15×32 channel, 250 kHz filter bank.

Observations were made in position-switching mode with reference positions $10'$ west of the map centers. The CS maps presented in Figure 1 as well as maps of the millimeter dust continuum emission (Launhardt et al. 1998b) clearly show that this throw is large enough to avoid CS emission in the reference beam (see Table 11). The single-sideband system temperature of the receiver array varied between 400 and 800 K during the observations. Typical rms noise was 0.03–0.05 K. Telescope pointing and focus were checked

TABLE 1

GLOBULES WITH *IRAS* POINT SOURCES

Source	Other Names	R.A.(1950)[a]	Decl.(1950)[a]	V_{LSR}(km s^{-1})	Lada Class	Remarks[b]	Telescopes
CB 3	LBN 594	00 25 59.0	56 25 32	−38.4	I[c,e]	1, 2	FCRAO, IRAM, CSO
CB 6	LBN 613	00 46 34.3	50 28 25	−12.4	I[c,d,e]	2	FCRAO, IRAM
CB 12	...	01 35 05.0	64 50 00	−11.4	...		FCRAO
CB 17	L1389	04 00 30.8	56 47 59	−4.7	(0)[c,d]	2	IRAM, CSO
CB 26	L1439	04 55 56.1	52 00 17	5.8	I[c]	2	IRAM
CB 28-2	LBN 923	05 03 44.5	−04 02 58	9.0	...		FCRAO
CB 29-2	...	05 19 28.0	−03 43 26	11.2	...		FCRAO
CB 30	...	05 26 51.9	05 38 15	0.6	II-D[e]		FCRAO
CB 32	LBN 921	05 33 47.5	−00 19 05	−5.0	II[c,e]		FCRAO
CB 34	...	05 44 02.8	20 59 07	0.5	I[c,d,e]	1, 2	FCRAO, SEST, CSO
CB 39	...	05 59 06.0	16 30 58	2.4	II[c,e]	1	FCRAO, SEST
CB 52	...	06 46 25.3	−16 50 38	16.8	II-D[c,e]	2	FCRAO, SEST
CB 54	LBN 1042	07 02 06.0	−16 18 47	19.7	I[c,d,e]	1, 2	FCRAO, IRAM, SEST, CSO
CB 58-1	...	07 15 56.2	−23 29 36	15.1	...		SEST
CB 58-2	...	07 16 09.1	−23 36 11	15.1	II-D[e]	2	SEST
CB 60-1	L1670	08 02 38.2	−31 22 09	13.9	II-D[c,e]		SEST
CB 68	L146	16 54 27.2	−16 04 48	5.5	(0)[c]	2	FCRAO
CB 81	L1774	17 19 22.9	−27 05 56	3.7	...	1	SEST
CB 82	B68, L55	17 19 34.0	−23 47 45	3.4	II[c]		FCRAO
CB 107-1	B86, L93	17 59 43.3	−27 54 37	10.7	II[e]		SEST
CB 114	...	18 09 18.6	−22 41 23	11.9	II[e]		SEST
CB 125-1	B92, L323	18 12 36.0	−18 20 15	6.4	...		SEST
CB 138	L414	18 22 09.4	−10 55 11	6.2	...		SEST
CB 142	...	18 27 12.1	−13 43 12	18.6	II[e]		FCRAO
CB 145	B100, L443	18 29 37.2	−09 11 40	4.5	II[e]		SEST
CB 184	L709	19 11 41.3	16 23 14	6.3	II[e]		IRAM
CB 188	...	19 17 54.0	11 29 56	6.8	I[c,e]	1, 2	FCRAO, IRAM
CB 192	L686	19 20 50.9	12 22 44	6.9	...		IRAM
CB 205	L810	19 43 21.7	27 43 37	15.3	I[c,e]	1, 2	IRAM
CB 214	L814	20 01 52.8	26 29 48	9.1	I[e]	1	FCRAO, IRAM
CB 216	L797	20 03 44.4	23 17 55	12.5	I[c,e]	1	FCRAO, IRAM
CB 222	L1094	20 32 49.9	63 52 00	0.1	I[e]		IRAM
CB 224	L1100	20 35 33.9	63 43 08	−2.7	I[c]	2	IRAM
CB 230	L1177	21 16 54.4	68 04 52	2.7	I[c,d,e]	1, 2	FCRAO, IRAM, CSO
CB 232	B158	21 35 14.4	43 07 05	12.5	I[c,e]	1, 2	FCRAO, IRAM, CSO
CB 240	L1192	22 31 45.9	58 16 26	−3.9	II-D[c,e]	2	FCRAO, IRAM
CB 243	L1246	23 22 52.9	63 20 04	−11.3	(0)[c,d]	2	FCRAO, IRAM
CB 244	L1262	23 23 48.8	74 01 08	4.2	(0)[c,d]	1, 2	FCRAO, IRAM, CSO
CB 247[f]	L1263	23 55 03.6	64 30 10	−3.7	II[e]	1	FCRAO

[a] All positions are from IPSC except CB 12 (YC92) and CB 82 (CB). Units of right ascension are hours, minutes, and seconds, and units of declination are degrees, arcminutes, and arcseconds.

[b] REMARKS.—(1) Outflow sources detected by YC92. (2) Detected at 1.3 mm continuum by LH97.

[c] Launhardt 1996.

[d] Launhardt et al. 1997.

[e] Yun & Clemens 1995.

[f] "Envelope-type" *IRAS* point source, i.e., outside the optical boundary of the globule.

TABLE 2

GLOBULES WITHOUT *IRAS* POINT SOURCES

Source	Other Names	R.A.(1950)	Decl.(1950)	V_{LSR} (km s^{-1})	Position Reference[a]	Remarks[b]	Telescopes
CB 13	L1345	01 53 16.0	62 31 36	35.9	YC		FCRAO
CB 44	B227, L1570	06 04 34.0	19 28 19	−0.3	CB		FCRAO
CB 64	LBN 37	15 57 35.0	−01 18 19	0.7	YC		FCRAO
CB 66	L121	16 36 41.0	−14 00 00	3.4	YC		FCRAO
CB 98	...	17 44 02.0	−20 29 26	10.7	CB	1	SEST
CB 217	L863	20 05 55.0	36 48 14	−0.5	YC	2	FCRAO
CB 231	B157	21 32 18.0	54 28 06	6.5	CB		FCRAO
CB 233	B161	21 39 00.0	57 34 26	−0.8	CB		FCRAO
CB 246	L1253	23 54 12.0	58 17 47	−0.5	CB	1	IRAM

NOTE.—Units of right ascension are hours, minutes, and seconds, and units of declination are degrees, arcminutes, and arcseconds.

[a] CB: Clemens & Barvainis 1988; YC: Yun & Clemens 1992.

[b] REMARKS.—(1) Detected at 1.3 mm continuum by LH97. (2) Outflow source detected by YC92.

TABLE 3

OBSERVING PARAMETERS

Line	Frequency (GHz)	Telescope	Beamwidth θ_b (arcsec)	Resolution ΔV (km s^{-1})	Efficiency η_{mb}
CS $J = 2 \rightarrow 1$	97.9810	FCRAO	55	0.75	0.60[a]
CS $J = 2 \rightarrow 1$	...	SEST	51	0.24	0.73[b]
CS $J = 2 \rightarrow 1$	...	IRAM	25	0.12	0.65[c]
$C^{34}S$ $J = 2 \rightarrow 1$.....	96.4130	IRAM	25	0.12	0.65[c]
CS $J = 3 \rightarrow 2$	146.9690	IRAM	17	0.16	0.65[c]
$C^{34}S$ $J = 3 \rightarrow 2$.....	144.6171	IRAM	17	0.16	0.65[c]
CS $J = 5 \rightarrow 4$	244.9356	IRAM	11	0.24	0.45[c]
CS $J = 5 \rightarrow 4$	...	CSO	30	0.15	0.72[d]

[a] M. Heyer, private communication.
[b] ESO Operating Manual No. 19, "The SEST Handbook" (1993).
[c] IRAM Newsletter No. 5 (1992).
[d] Mangum 1993.

every 2 or 3 hr by observing T Cep and IK Tau in the SiO $v = 1$, $J = 2 \rightarrow 1$ maser line (86.244 GHz) or observing planets in the continuum mode. Pointing was repeatable to 7″ (rms). Data reduction included removing linear baselines and eliminating occasional spikes from the spectra.

2.2.2. *SEST Observations*

The CS $J = 2 \rightarrow 1$ line was observed toward 14 globules (including two positions in CB 58) with the 15 m SEST telescope on La Silla, Chile in 1992 October. A 3 mm Schottky receiver was used in the single-sideband mode with a typical system temperature of 350 K during the observations. An acousto-optical spectrometer (AOS) with 2000 channels, a total bandwidth of 86 MHz, and a channel separation of 43 kHz served as backend. The SEST observations have spatial resolution similar to the FCRAO observations but have better velocity resolution (see Table 3). The observations were made in the symmetric beam-switching mode with reference positions $\pm 11\farcm6$ in azimuth from the source position. Typical rms noise level was 0.04–0.06 K. Telescope pointing was checked regularly by observing Orion A in the SiO maser line at 86 GHz; it was repeatable to 6″ (rms).

2.2.3. *IRAM Observations*

The IRAM CS and $C^{34}S$ observations toward 18 globules were made during 1993 June. Three SIS receivers, operating at 3 mm, 2 mm, and 1 mm, were used simultaneously. Typical system temperatures during the observations were 230–300 K at 96 and 98 GHz, 200–350 K at 145 and 147 GHz, and about 550 K at 245 GHz. Two autocorrelators with channel widths of 40 and 80 kHz at 100 and 150 GHz, respectively, and a 256 channel, 100 kHz filter bank at 245 GHz were used.

The observations were made in the position switching mode with reference positions 20′ east of the source positions. The typical rms noise was 0.12 K for $J = 2 \rightarrow 1$ and 0.08 K for $J = 3 \rightarrow 2$. The telescope pointing and focus were checked typically every 2 hr toward W3(OH) and K3-50A. The pointing was repeatable to 5″ (rms). In addition to the standard calibration method, the calibration was checked by monitoring the secondary standards W3(OH), W51E, DR 21, and Ori IRc2 (Mauersberger et al. 1989).

Each of the 18 sources was observed simultaneously in the CS $J = 2 \rightarrow 1$ and $J = 3 \rightarrow 2$ lines toward the center position, and small maps were made of a few sources. Single spectra in the $C^{34}S$ $J = 2 \rightarrow 1$, $C^{34}S$ $J = 3 \rightarrow 2$, and the CS $J = 5 \rightarrow 4$ lines were obtained toward the peak positions of the strongest sources.

2.2.4. *CSO Observations*

The CS $J = 5 \rightarrow 4$ line was observed using the CSO[8] 10 m telescope toward the centers of eight globules during runs in 1992 December and 1993 February, August, and October. An SIS receiver was used in double-sideband mode with a typical system temperature of 300 K. Observations were carried out in position-switching mode with reference positions 10′ west of the sources. Typical rms noise was 0.03 K. The spectrometer was an acousto-optical spectrometer with 1024 channels and a total bandwidth of 50 MHz. Telescope pointing was checked by observing planets and the pointing was better than 5″ (rms) during the observations.

3. RESULTS

3.1. CS $J = 2 \rightarrow 1$ Results

3.1.1. *Detection Rates*

The results of the CS $J = 2 \rightarrow 1$ survey are summarized in Tables 4, 5, and 6. The detection statistics are summarized in Table 7. With the sensitivities of the survey (1 σ), typically < 0.05 K at FCRAO and at SEST, and 0.1 K at IRAM, 32 of the 47 globules were detected above the 3 σ level in the CS $J = 2 \rightarrow 1$ line. This corresponds to an overall detection rate of 68%.

The detection rates for globules with and without *IRAS* point sources are 72% (28 of 39 sources) and 44% (four of nine globules), respectively. Two of the detections in the latter group are in CB 98 and CB 246, which were also detected in the 1.3 mm continuum (LH97). If we set a threshold of $\int T_{mb}\, dv \geq 1$ K km s^{-1}, 13 of 39 (33%) globules with *IRAS* sources achieve this, while only one (CB 246) of nine (11%) of those without *IRAS* sources do. Like HCN (Afonso et al. 1998), CS is much more readily detected and stronger when detected toward cores with *IRAS* sources than toward "starless" cores.

Among the globules associated with *IRAS* point sources, there are differences between the detection rates of the sources assigned to different classes. The detection rates for Class 0 and Class I sources (100% in each group) are much higher than that for all other sources (all about 50%).

[8] The CSO is operated by the California Institute of Technology under funding from the National Science Foundation, contract AST 93-13929.

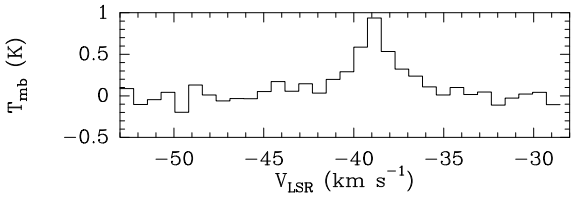

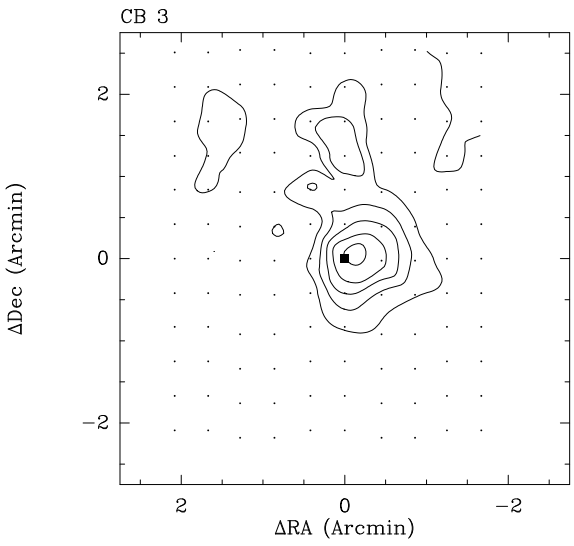

FIG. 1*a*

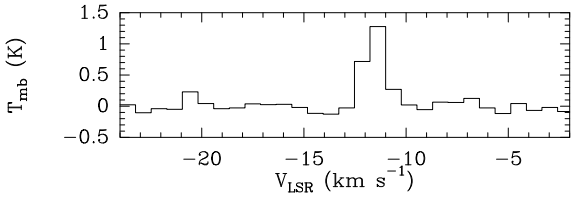

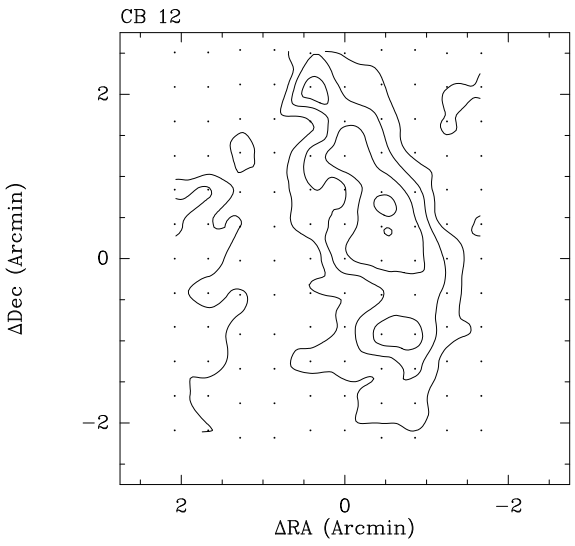

FIG. 1*b*

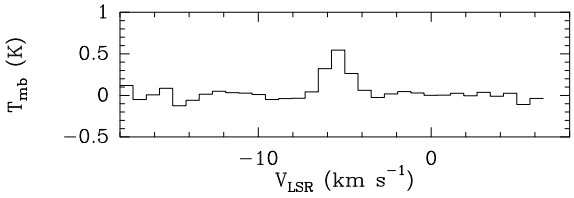

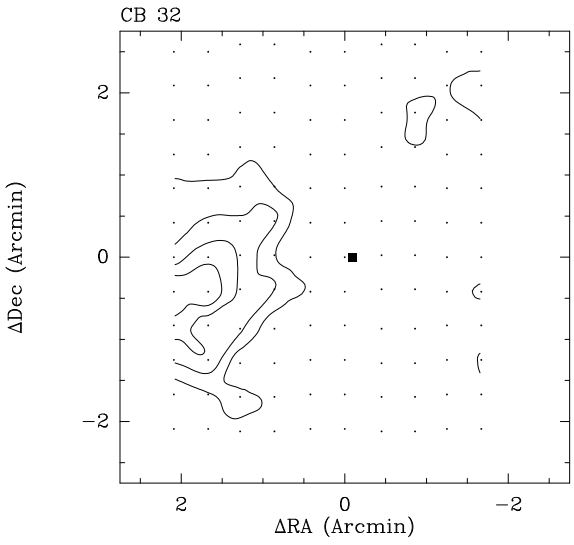

FIG. 1*c*

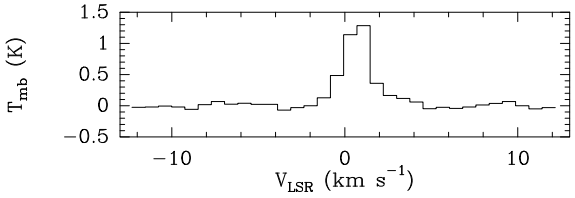

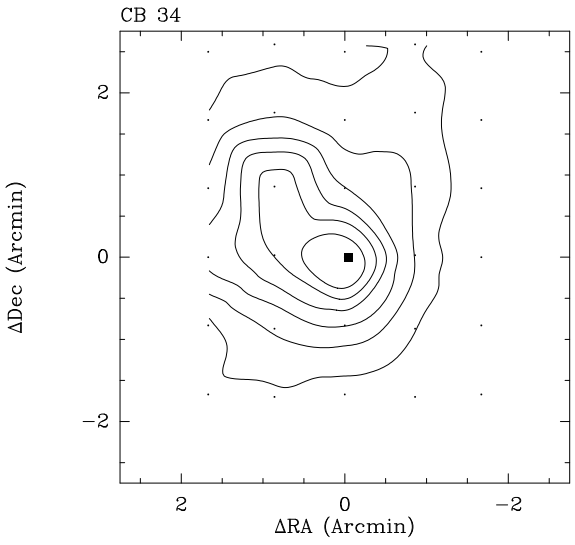

FIG. 1*d*

FIG. 1.—For each of 12 sources mapped at FCRAO, there are two panels. The upper panel shows the spectrum on the T_{mb} scale. The lower panel shows a map of integrated intensity (again on T_{mb} scale), along with the locations of the grid of spectra (*small dots*) and the location of the *IRAS* source (*filled square*). The contours are drawn at the following intervals: (*a*) 0.50 to 2.5 by 0.50 K km s^{-1} (CB 3, 3 σ); (*b*) 0.42 to 1.7 by 0.42 K km s^{-1} (CB 12, 3 σ); (*c*) 0.25 to 1.0 by 0.25 K km s^{-1} (CB 32, 2 σ); (*d*) 0.42 to 2.5 by 0.42 K km s^{-1} (CB 34, 4 σ); (*e*) 0.25 to 0.75 by 0.25 K km s^{-1} (CB 44, 2 σ); (*f*) 0.33 to 2.0 by 0.33 K km s^{-1} (CB 54, 2 σ); (*g*) 0.42 to 0.84 by 0.42 K km s^{-1} (CB 68, 3σ); (*h*) 0.22 to 0.44 by 0.22 K km s^{-1} (CB 216, 2 σ); (*i*) 0.13 to 0.39 by 0.13 K km s^{-1} (CB 230, 2 σ); (*j*) 0.17 to 0.67 by 0.17 K km s^{-1} (CB 232, 2 σ); (*k*) 0.25 to 0.75 by 0.25 K km s^{-1} (CB 243, 2 σ); (*l*) 0.17 to 0.85 by 0.17 K km s^{-1} (CB 244, 2 σ).

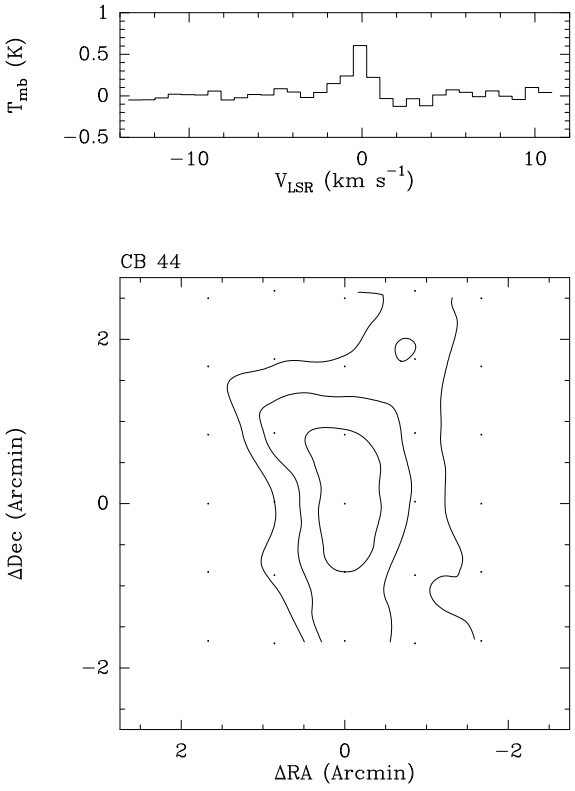

FIG. 1*e*

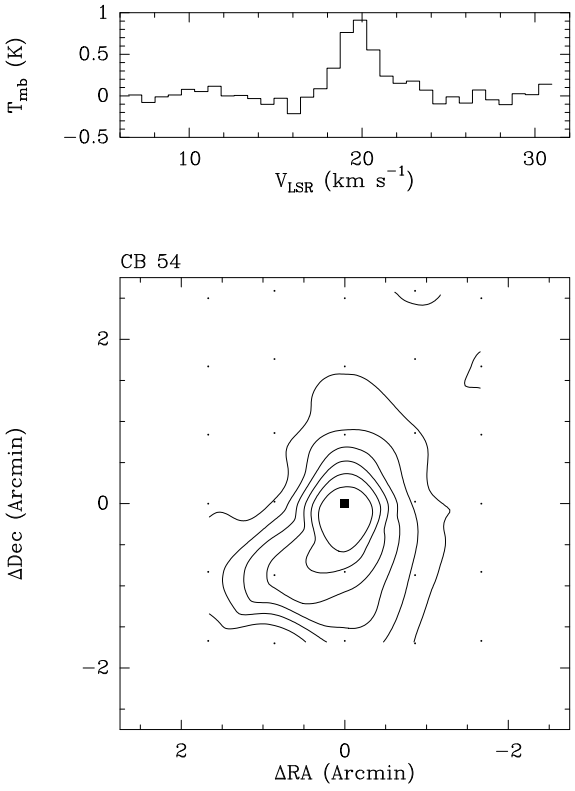

FIG. 1*f*

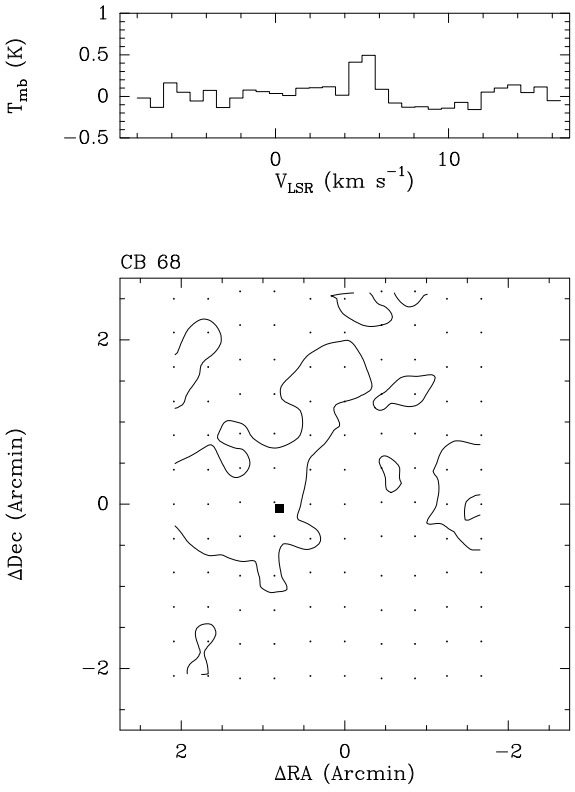

FIG. 1*g*

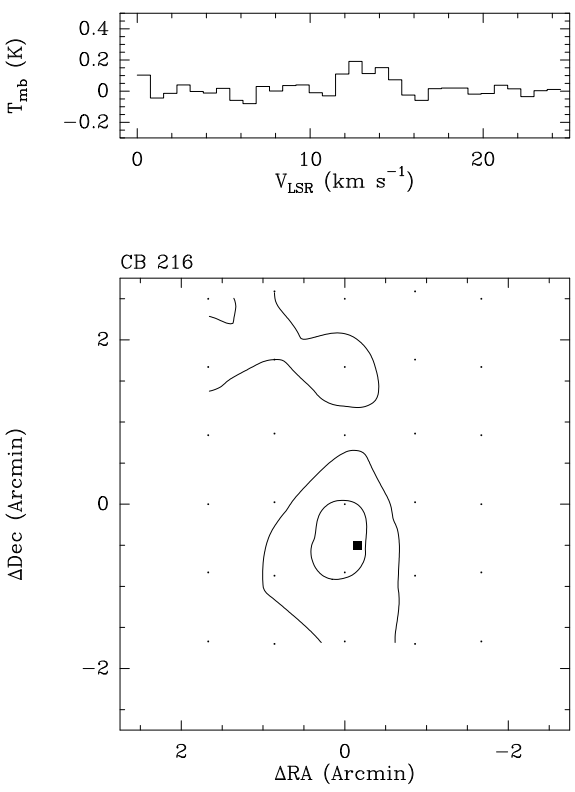

FIG. 1*h*

Applying the above threshold of 1 K km s^{-1}, 100% of the Class 0 sources (four of four sources) and 54% of the Class I sources (seven of 13 sources) have strong CS emission. In contrast, none of the Class II-D and Class II sources were found to have strong CS emission. Owing to the small number of Class 0 and II-D sources observed in the survey and owing to the uncertainties in the classification described in § 2.1, these differences should not be overinter-

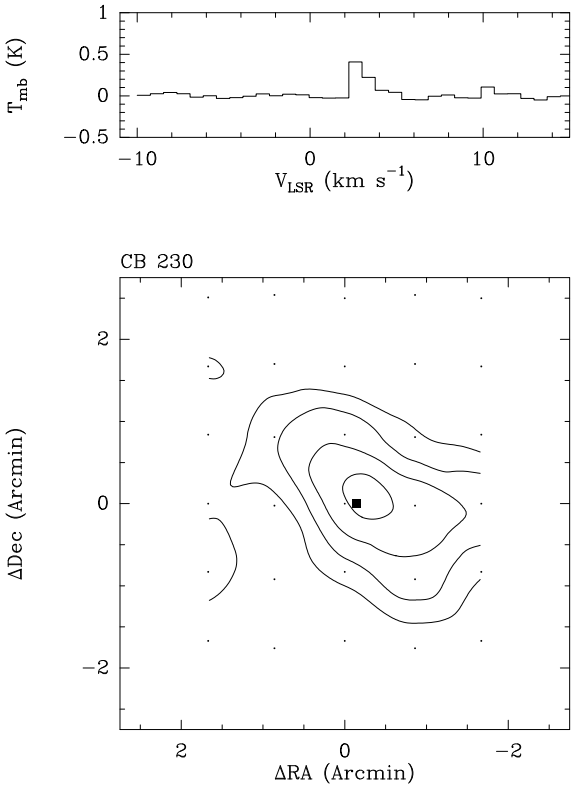

FIG. 1*i*

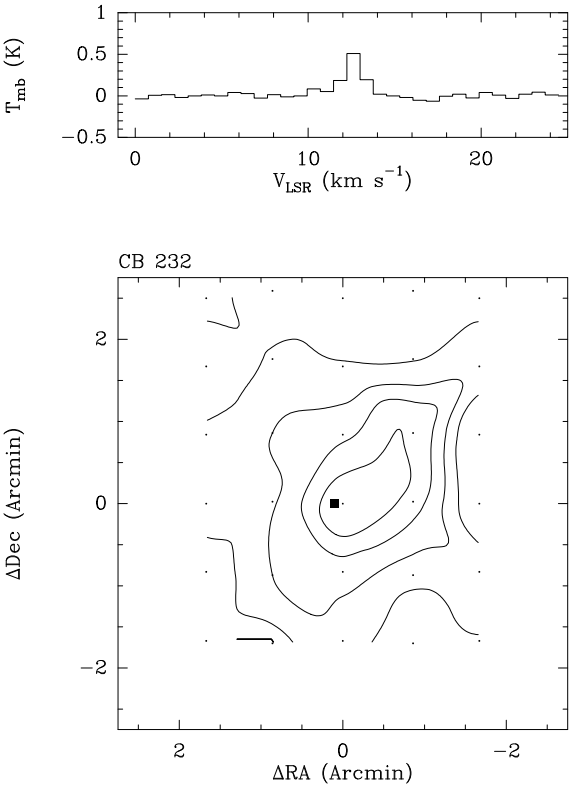

FIG. 1*j*

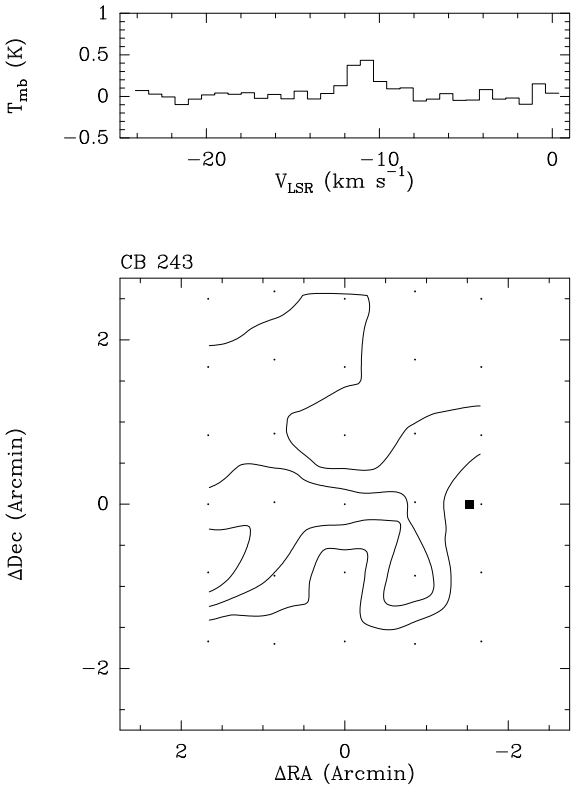

FIG. 1*k*

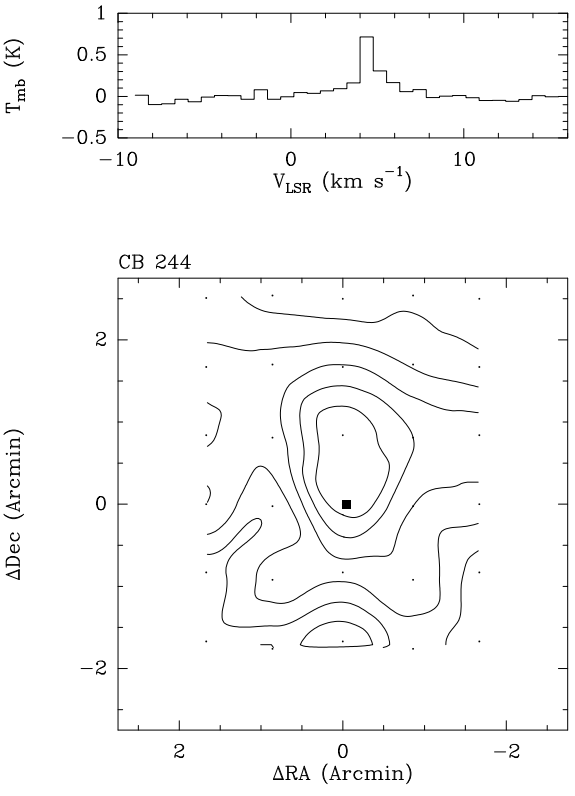

FIG. 1*l*

preted.

The detection rate for outflow sources is 79% (11 of 14 globules). Two of the three outflow sources with no detectable CS emission, CB 81 and CB 247, were only marginally detected in the $C^{18}O$ $J = 2 \rightarrow 1$ line (WEZC95), while the remaining outflow source, CB 217, had moderately strong $C^{18}O$ $J = 2 \rightarrow 1$ emission. These outflow sources should be reexamined to ascertain whether they indeed have low column densities (or abundances) in common tracers such as $C^{18}O$ and CS.

All but two sources detected in the 1.3 mm continuum survey (LH97) were also detected in the CS $J = 2 \rightarrow 1$

TABLE 4

RESULTS OF THE FCRAO CS $J = 2 \rightarrow 1$ SURVEY

	Map Center		Peak					
Source	R.A.(1950)	Decl.(1950)	$\Delta\alpha$ (arcmin)	$\Delta\delta$ (arcmin)	T_{mb}[a] (K)	$\int T_{mb}\, dv$[b] (K km s^{-1})	V_{LSR}	Line Width[c] ΔV (km s^{-1})
CB 3	00 25 59	56 25 32	0.0	0.0	0.93 ± 0.13	2.50 ± 0.20	-38.9 ± 0.2	2.6
CB 6	00 46 34	50 28 25	...	...	<0.30	...	...	...
CB 12	01 35 05	64 50 00	-0.5	0.8	1.28 ± 0.08	1.62 ± 0.17	-11.6 ± 0.2	1.3
CB 13	01 53 16	62 31 36	...	...	<0.25	...	...	...
CB 28	05 03 45	-04 02 58	1.3	2.6	0.93 ± 0.08	1.27 ± 0.18	...	1.4
CB 29	05 19 34	-03 43 56	1.7	0.0	0.43 ± 0.05	0.58 ± 0.05	...	1.3
CB 30	05 26 52	05 38 15	0.0	0.0	0.27 ± 0.08	0.48 ± 0.13	...	1.8
CB 32	05 33 48	-00 19 05	1.7	0.0	0.55 ± 0.05	0.92 ± 0.10	-5.4 ± 0.2	1.7
CB 34	05 44 03	20 59 07	0.0	0.0	1.28 ± 0.05	2.83 ± 0.08	0.9 ± 0.3	2.2
CB 39	05 59 06	16 30 58	0.0	0.8	0.17 ± 0.05	0.40 ± 0.08	...	2.4
CB 44	06 04 32	19 28 19	0.0	0.0	0.60 ± 0.05	0.90 ± 0.10	-0.1 ± 0.2	1.5
CB 52	06 46 25	-16 50 38	...	...	<0.20	...	...	...
CB 54	07 02 06	-16 18 47	0.0	0.0	0.92 ± 0.07	2.37 ± 0.17	19.7 ± 0.3	2.6
CB 64	16 57 35	-01 18 19	...	...	<0.35	...	...	...
CB 66	16 36 41	-14 00 00	...	...	<0.25	...	...	...
CB 68	16 54 24	-16 04 45	0.0	1.7	0.50 ± 0.10	0.72 ± 0.15	5.3 ± 0.3	1.5
CB 82	17 19 34	-23 47 45	0.9	1.8	0.22 ± 0.07	0.37 ± 0.08	...	1.7
CB 142.....	18 27 10	-13 42 51	...	...	<0.25	...	...	...
CB 188.....	19 17 57	11 30 18	0.5	0.0	0.48 ± 0.07	0.42 ± 0.12	...	0.9
CB 214.....	20 01 54	26 29 42	...	...	<0.25	...	...	...
CB 216.....	20 03 45	23 18 25	0.0	-0.8	0.20 ± 0.03	0.45 ± 0.07	12.7 ± 1.0	2.3
CB 217.....	20 05 55	36 48 14	...	...	<0.50	...	...	...
CB 230.....	21 16 55	68 04 52	0.0	0.0	0.42 ± 0.03	0.52 ± 0.05	2.9 ± 0.3	1.3
CB 231.....	21 32 18	54 28 06	...	...	<0.20	...	...	...
CB 232.....	21 35 14	43 07 05	0.0	0.0	0.52 ± 0.05	0.77 ± 0.07	12.7 ± 0.2	1.5
CB 233.....	21 39 00	57 34 26	-0.9	0.0	0.18 ± 0.05	0.30 ± 0.07	...	1.6
CB 240.....	21 31 46	58 17 26	...	...	<0.20	...	...	...
CB 243.....	23 22 59	63 20 04	1.7	-0.8	0.47 ± 0.07	0.92 ± 0.08	-10.8 ± 0.3	2.1
CB 244.....	23 23 49	74 01 08	0.0	0.0	0.72 ± 0.05	1.08 ± 0.07	4.6 ± 0.3	1.5
CB 247.....	23 55 04	64 30 10	...	...	<0.15	...	...	...

NOTE.—Units of right ascension are hours, minutes, and seconds, and units of declination are degrees, arcminutes, and arcseconds.

[a] Peak intensity.

[b] Integrated intensity.

[c] $\Delta V = \int T_{mb}\, dv / T_{mb}$.

TABLE 5

THE SEST CS $J = 2 \rightarrow 1$ LINE PARAMETERS

	Offsets		CS $J = 2 \rightarrow 1$				
Source	$\Delta\alpha$ (arcsec)	$\Delta\delta$ (arcsec)	T_{mb} (K)	$\int T_{mb}\, dv$ (K km s^{-1})	V_{LSR} (K km s^{-1})	ΔV(K km s^{-1})	Line Shape[a]
CB 34	0	0	1.86 ± 0.08	3.56	0.56 ± 0.02	1.73 ± 0.04	w2
CB 39	0	0	<0.16	...	...	...	...
CB 52	0	0	0.16 ± 0.05	0.32	15.88 ± 0.07	1.44 ± 0.23	sa,u
CB 54	0	0	1.74 ± 0.07	4.10	19.62 ± 0.01	2.08 ± 0.04	b
CB 58-1	0	0	<0.25	...	...	...	...
CB 58-2	0	0	0.68 ± 0.07	0.96	14.96 ± 0.04	1.26 ± 0.09	g
CB 60	0	0	<0.16	...	...	...	...
CB 68	0	0	0.83 ± 0.05	1.04	4.95 ± 0.04	1.28 ± 0.08	g
CB 81	0	0	<0.25	...	...	...	...
CB 98	0	0	1.01 ± 0.12	0.68	10.68 ± 0.03	0.61 ± 0.06	g
CB 107-1.....	0	0	<0.25	...	...	...	...
CB 114	0	0	<0.29	...	...	...	...
CB 125-1.....	0	0	0.37 ± 0.05	0.33	6.29 ± 0.03	0.84 ± 0.09	g
CB 138	0	0	<0.25	...	...	...	...
CB 145	0	0	<0.25	...	...	...	...

NOTE.—Line parameters are derived from Gaussian fits (see § 3.1.2).

[a] g = Gaussian profile; w2 = red and blue wing; sa = (symmetric) self-absorption; b = blue asymmetry; u = uncertain (fit depends on masking).

TABLE 6

THE IRAM CS $J = 2 \rightarrow 1$ LINE PARAMETERS

SOURCE	OFFSETS		CS $J = 2 \rightarrow 1$				
	$\Delta\alpha$ (arcsec)	$\Delta\delta$ (arcsec)	T_{mb} (K)	$\int T_{mb}\, dv$ (K km s^{-1})	V_{LSR} (km s^{-1})	ΔV (km s^{-1})	Line Shape[a]
CB 6	0	0	1.78 ± 0.14	1.05	−12.33 ± 0.01	0.48 ± 0.03	wb
CB 17	0	0	3.00 ± 0.14	1.69	−4.69 ± 0.01	0.51 ± 0.01	b
CB 26	0	0	1.42 ± 0.14	0.28	5.76 ± 0.04	0.51 ± 0.11	g
CB 54	0	0	3.08 ± 0.34	6.46	19.66 ± 0.03	2.03 ± 0.07	b
CB 184.....	0	0	0.77 ± 0.20	0.17	6.15 ± 0.02	0.18 ± 0.07	...
CB 188.....	0	0	0.76 ± 0.21	0.98	6.58 ± 0.03	1.00 ± 0.09	sa,u
CB 192.....	0	0	<0.75	...	...	...	...
CB 205.....	0	0	2.30 ± 0.14	3.38	15.69 ± 0.01	1.21 ± 0.04	w2
CB 214.....	0	0	1.00 ± 0.18	0.66	9.23 ± 0.04	0.87 ± 0.07	b,u
CB 216.....	0	0	0.62 ± 0.20	0.65	12.28 ± 0.03	0.80 ± 0.08	sa
CB 222.....	0	0	1.54 ± 0.14	0.74	−2.74 ± 0.01	0.43 ± 0.03	g
CB 224.....	0	0	1.30 ± 0.17	1.10	−2.56 ± 0.03	1.05 ± 0.12	b,u
CB 230.....	−20	0	2.46 ± 0.23	1.37	2.73 ± 0.02	0.56 ± 0.04	b,u
CB 232.....	0	12	2.49 ± 0.18	2.77	12.39 ± 0.01	0.84 ± 0.03	wb
CB 240.....	0	0	<0.65	...	...	...	...
CB 243.....	0	12	1.48 ± 0.11	1.54	−11.13 ± 0.01	1.02 ± 0.03	g
CB 244.....	−12	0	1.94 ± 0.15	2.77	4.14 ± 0.02	0.98 ± 0.07	r, w2
CB 246.....	−20	−40	1.80 ± 0.17	1.00	−0.73 ± 0.01	0.52 ± 0.03	g

NOTE.—Line parameters are derived from Gaussian fits (see § 3.1.2).

[a] g = Gaussian profile; sa = (symmetric) self-absorption; b = blue asymmetry; r = red asymmetry; wb = blue wing; w2 = red and blue wing; u = uncertain (fit depends on masking).

survey. The two exceptions (CB 145 and CB 240) have only weak 1.3 mm continuum emission, detected at the 4–5 σ level.

3.1.2. *Emission Strengths and Line Shapes*

Since the velocity resolution of the FCRAO observations was 0.75 km s^{-1}, most of the CS lines are only barely resolved. Consequently, the peak line temperatures are likely to be underestimated, but the integrated intensities should be more accurate. The line widths (ΔV) for the FCRAO data in Table 4 were derived by dividing the integrated intensity ($\int T_{mb}\, dv$) by the measured peak line temperature (T_{mb}). Figure 1 shows the CS $J = 2 \rightarrow 1$ peak spectra of 12 sources (together with the maps) observed with the FCRAO. The values of T_{mb} and ΔV for the SEST and IRAM spectra were derived from Gaussian fits to the lines after masking out wings and self-absorption features. When the result depended strongly on the masking region, a "u" is used to indicate the uncertainty.

Comparison of the emission strength and line widths measured with the three telescopes is difficult. Most of the IRAM data were taken at positions that differed from the positions measured with the FCRAO. The only exception is CB 54, which was observed at all three telescopes toward the same position. There are, however, eight sources for which the positions observed at IRAM differ less than one FCRAO beam from the FCRAO positions. Comparing these sources and the three sources that were observed at both FCRAO and SEST, the average ratios between the FCRAO, SEST, and IRAM spectra are 1:1.6:3 for peak line temperatures, and 1:1.5:2 for integrated intensities (corrected for efficiencies). Since the beams of FCRAO and SEST are very similar, the factor of 1.5 likely represents calibration differences. All globules considered here have *IRAS* point sources. The larger values for the IRAM data probably reflect the smaller beam size. Higher intensities in the smaller beam can reflect small scale structure, such as, e.g., a density and temperature gradient. In CB 54, the only source observed at all three telescopes, the line width decreases with decreasing beam size. Comparison of the average line widths of all globules with *IRAS* point sources observed at the three telescopes results in the same trend (FCRAO:SEST:IRAM = 1.8 ± 0.5:1.7 ± 0.3:1.0 ± 0.4 km s^{-1}). Because of these differences in calibration, peak position, and effects of source structure, we will mostly focus on detection rates, line profiles, and map morphology, rather than quantitative measures of intensity.

We characterized the line shapes of the SEST and IRAM spectra and listed the results in Tables 5 and 6. The note "g" means that the profile is Gaussian; "wb" means that a

TABLE 7

DETECTION STATISTICS FOR THE CS $J = 2 \rightarrow 1$ SURVEY

Class	Total	Detected	Rate (%)	Strong[a]	Rate (%)
0	4	4	100	4	100
I.....	13	13	100	7	54
II-D.....	5	3	60	0	0
II.....	9	4	44	0	0
No classification	8	4	50	2	25
All with *IRAS* source.....	39	28	72	13	33
"Starless" globules	9	4	44	1	11

[a] $\int T_{mb}\, dv \geq 1$ K km s^{-1}.

blue wing is apparent (e.g., CB 232, Fig. 2*c*), and "w2" means both red and blue wings are seen (e.g., CB 244, Fig. 2*d*); "sa" denotes a symmetric self-absorption feature, while "b" indicates that the line is skewed to the blue (e.g., CB 54, Fig. 2*a*), and "r" means that it is skewed to the red. Especially in the small IRAM beam, most lines have non-Gaussian profiles. Line wings were seen in the spectra of CB 34, CB 205, CB 232, and CB 244, which all have CO outflows (YC92). In addition, we found a blue CS line wing in CB 6, in which no CO outflow has been detected yet. Self-absorption features were found in the CS $J = 2 \rightarrow 1$ lines of eight globules (all with Class 0 or I sources). The line center velocities were checked with the optically thin $C^{34}S$ lines or with the $C^{18}O$ lines (WEZC95) to rule out the alternative possibility of two velocity components.

3.1.3. *FCRAO Maps*

Twenty-five globules with *IRAS* sources and five "starless" globules were mapped in the CS $J = 2 \rightarrow 1$ line at the FCRAO. Nineteen (15 *IRAS* globules and four "starless" globules) showed detectable (>3 σ) CS $J = 2 \rightarrow 1$ emission within the mapped region. Figure 1 shows maps and the peak spectra in 12 sources, with the locations of *IRAS* point sources marked as filled squares.

Table 4 lists the line parameters of all 30 globules at the position of peak emission. In the case of CB 68, the peak is very ill defined (there are lines nearly as strong closer to the *IRAS* source), and the morphology depends strongly on the contour levels.

Four globules (CB 28, CB 29, CB 32, and CB 243) have CS emission peaking $>1'$ (~ 1 FWHM beam) away from the *IRAS* point sources. Since the SEST and IRAM observations were carried out mostly as single-point observations, the fact that some globules have CS emission peaking away from the *IRAS* point sources suggests that a survey with broader coverage of the globules would increase the CS detection rate.

Nine other sources have CS emission peaks located within $1'$ of the *IRAS* sources; prominent emission peaks are seen at the *IRAS* sources in seven globules: CB 3, CB 34, CB 54, CB 216, CB 230, CB 232, and CB 244. These sources also showed prominent cores in $C^{18}O$ $J = 2 \rightarrow 1$ maps (WEZC95), have CO outflows (YC92) and (except CB 216) were detected at 1.3 mm continuum (LH97) as well as in the H_2CO $J_{K-1K_1} = 3_{12} \rightarrow 2_{11}$ line (WEZC95), which also traces dense gas. Six of these sources were classified as Class I sources, and CB 244 was classified as a Class 0 source (Table 1). In summary, the *IRAS* point sources

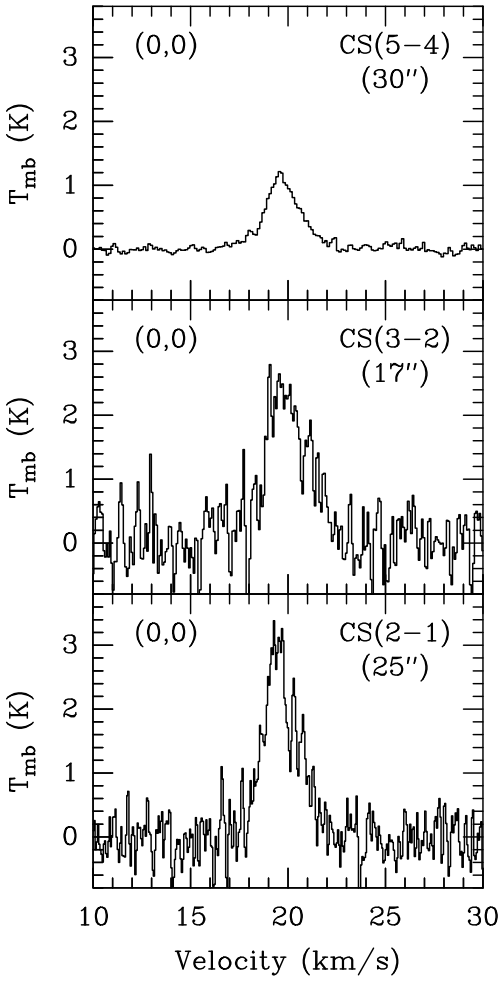

FIG. 2*a*

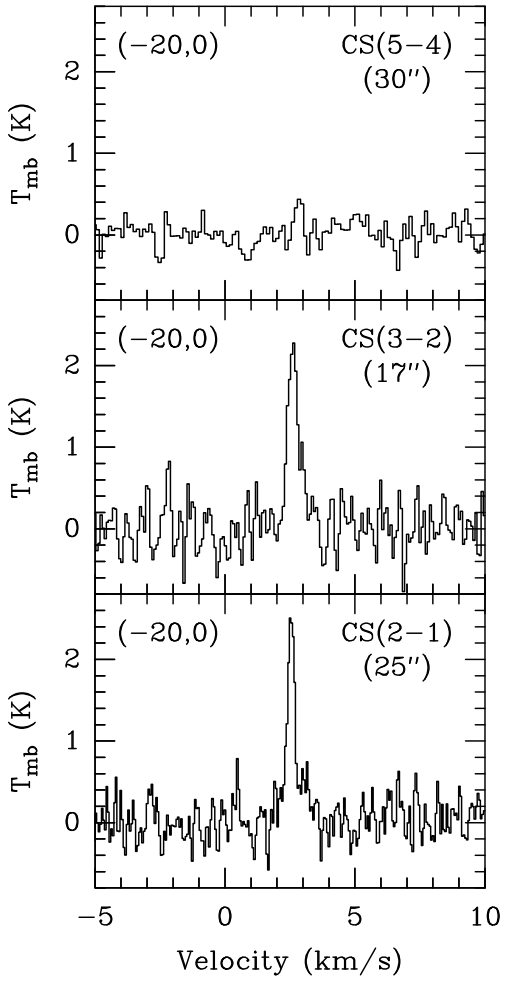

FIG. 2*b*

FIG. 2.—For each of four sources, the spectra from IRAM and the CSO are shown. (*a*) CB 54; (*b*) CB 230; (*c*) CB 232; (*d*) CB 244. Note that the positions of the CS $J = 5 \rightarrow 4$ spectra from IRAM and the CSO are different for CB 244. The observed line and the beam sizes are marked in the upper right-hand corner of the spectra boxes and the observed positions in the upper left-hand corner.

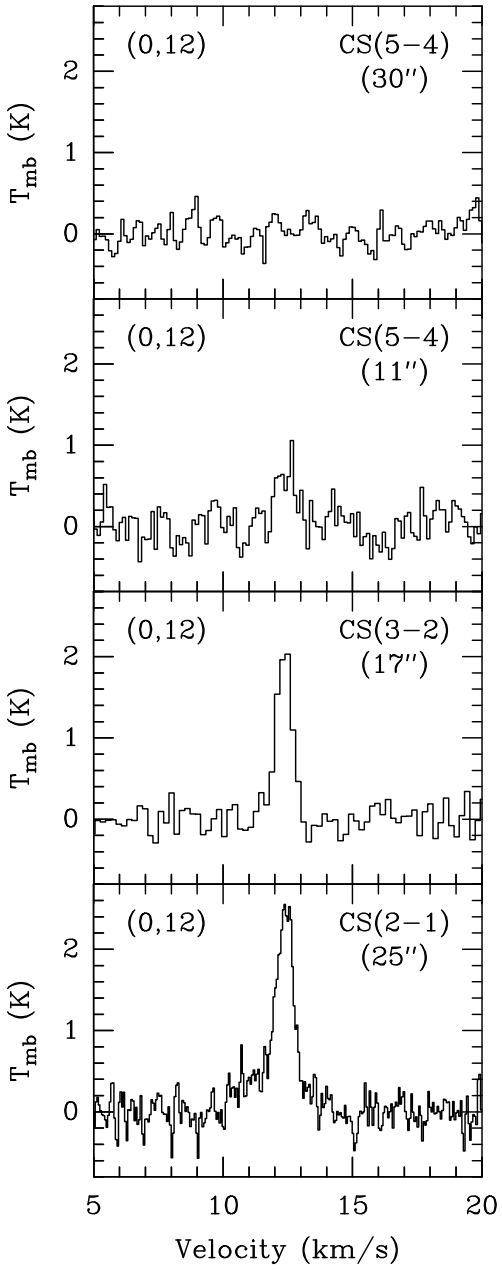

FIG. 2*c*

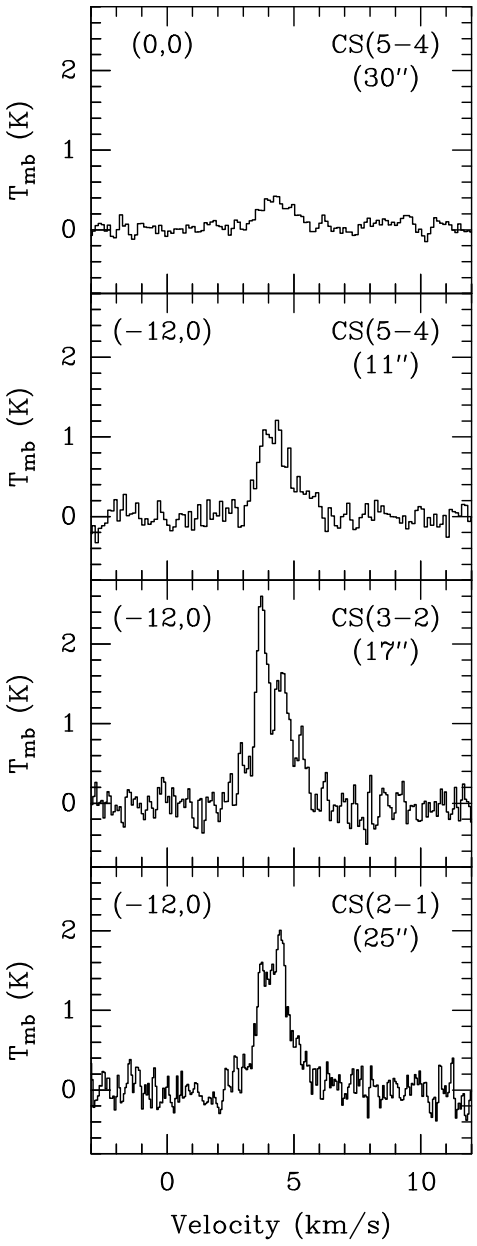

FIG. 2*d*

associated with the seven bright CS cores are likely to be very young stellar objects embedded in dense molecular cloud cores.

3.2. *Detection of Higher J Lines*

Of the 19 globules observed in higher J lines, 13 were detected at IRAM in the CS $J = 3 \rightarrow 2$ transition (Table 8), and eight were detected at either IRAM or the CSO in the $J = 5 \rightarrow 4$ line (Tables 8 and 9). Upper limits are 3 σ. Figure 2 shows the spectra in CB 54, CB 230, CB 232, and CB 244. Note that the positions of the spectra from IRAM and the CSO are different for CB 244.

3.3. *Isotopic Data*

Four of seven sources observed in the $C^{34}S$ $J = 2 \rightarrow 1$ and $C^{34}S$ $J = 3 \rightarrow 2$ lines at IRAM were detected (Table 10). Comparisons of the isotopic line intensities yield estimates of the CS line opacities. Assuming equal excitation temperatures and a terrestrial abundance ratio of 22 for $CS/C^{34}S$, optical depths of 3–5 for the CS $J = 2 \rightarrow 1$ line, and 1–9 for the $J = 3 \rightarrow 2$ line are derived. The line opacities for CB 6, CB 232, and CB 243 are less than 2–4, since $C^{34}S$ lines were not detected.

4. DISCUSSION

4.1. *Comparison to Other Tracers*

The overall detection rate (68%) for the CS $J = 2 \rightarrow 1$ line is identical to the detection rate for the $C^{18}O$ $J = 2 \rightarrow 1$ emission (68%) (WEZC95). Figure 3 plots for 21 sources the integrated intensities of the CS $J = 2 \rightarrow 1$ line versus the integrated intensities of the $C^{18}O$ $J = 2 \rightarrow 1$ line. The $C^{18}O$ data were converted to main-beam brightness temperature. Some sources are plotted more than once, and the points are coded by the telescope used. Globules with large total

TABLE 8

THE IRAM CS $J = 3 \rightarrow 2$ AND $J = 5 \rightarrow 4$ LINE PARAMETERS

	OFFSETS		CS $J = 3 \rightarrow 2$				CS $J = 5 \rightarrow 4$			
SOURCE	$\Delta\alpha$ (arcsec)	$\Delta\delta$ (arcsec)	T_{mb} (K)	$\int T_{mb}\, dv$ (K km s^{-1})	V_{LSR} (km s^{-1})	ΔV (km s^{-1})	T_{mb}	$\int T_{mb}\, dv$ (K km s^{-1})	V_{LSR} (km s^{-1})	ΔV (km s^{-1})
CB 6	0	0	1.02 ± 0.09	0.62	-12.28 ± 0.02	0.57 ± 0.04	<0.40	...	...	...
CB 17	0	0	2.15 ± 0.18	1.54	-4.70 ± 0.01	0.70 ± 0.03	0.40 ± 0.13	0.33	-4.57 ± 0.10	0.45 ± 0.26[b]
CB 26	0	0	0.57 ± 0.12	0.40	5.60 ± 0.06	0.68 ± 0.13	...	...	...	...
CB 54	0	0	2.31 ± 0.43	5.38	19.99 ± 0.06	2.67 ± 0.14[a]	...	...	...	...
CB 184.....	0	0	<0.37	...	...	...	...	...	...	...
CB 188.....	0	0	0.40 ± 0.12	0.62	6.36 ± 0.08	1.32 ± 0.22	...	...	...	...
CB 192.....	0	0	<0.26	...	...	...	...	...	...	...
CB 205.....	0	0	2.38 ± 0.11	6.00	15.82 ± 0.02	1.47 ± 0.05[a]	...	...	...	...
CB 214.....	0	0	0.34 ± 0.08	0.28	9.03 ± 0.05	0.57 ± 0.24	...	...	...	...
CB 216.....	0	0	0.54 ± 0.10	0.35	12.19 ± 0.09	0.93 ± 0.36	...	...	...	...
CB 222.....	0	0	1.31 ± 0.09	0.78	-2.75 ± 0.02	0.75 ± 0.06	...	...	...	...
CB 224.....	0	0	0.72 ± 0.09	0.74	-2.60 ± 0.04	0.85 ± 0.10 [ab]	...	...	...	...
CB 230.....	-20	0	2.15 ± 0.28	1.30	2.67 ± 0.02	0.56 ± 0.04[a]	...	...	...	...
CB 232.....	0	12	2.08 ± 0.14	1.69	12.36 ± 0.02	0.71 ± 0.04	0.71 ± 0.20	0.67	12.46 ± 0.06	0.89 ± 0.14
CB 240.....	0	0	<0.23	...	...	...	...	...	...	...
CB 243.....	0	12	1.49 ± 0.14	1.69	-11.18 ± 0.02	1.06 ± 0.04	...	...	...	...
CB 244.....	-12	0	2.54 ± 0.17	3.25	4.08 ± 0.01	1.02 ± 0.05[a]	1.07 ± 0.11	1.67	4.18 ± 0.03	1.31 ± 0.08
CB 246.....	-20	-40	1.92 ± 0.22	0.92	-0.74 ± 0.01	0.40 ± 0.04	<0.40	...	...	...

NOTE.—Line parameters are derived from Gaussian fits (see § 3.1.2).
[a] Non-Gaussian profiles.
[b] Fit depends strongly on masking.

column densities, as measured by the $C^{18}O$ data, also tend to have high CS integrated intensities, though there is considerable scatter. For the FCRAO data, the correlation coefficient between the CS and $C^{18}O$ integrated intensities is 0.64. Using robust estimation, the best-fitting linear relation has a slope of 0.36, while χ^2 fitting gives a slope of 0.63. The mean ratio of CS to $C^{18}O$ integrated intensities is 0.79 ± 0.48 for the FCRAO data and 1.31 ± 0.62 for the IRAM data, which reflects the stronger lines in the smaller beam of the IRAM data (see § 3.1.2). This behavior is expected for centrally condensed sources.

In the middle panel of Figure 3, the ratio of line widths, both corrected for instrumental broadening, is plotted versus the integrated intensity of $C^{18}O$. The FCRAO data are likely to overestimate the line width in sources in which the resolution was inadequate to resolve the line. In the six

TABLE 9

THE CSO CS $J = 5 \rightarrow 4$ LINE PARAMETERS

	OFFSETS		CS $J = 5 \rightarrow 4$			
SOURCE	$\Delta\alpha$	$\Delta\delta$	T_{mb}(K)	$\int T_{mb}\, dv$(K km s^{-1})	V_{LSR}(km s^{-1})	ΔV(km s^{-1})
CB 3	-18	0	0.71 ± 0.08	4.17 ± 0.14	-38.59 ± 0.07	5.48 ± 0.24[a]
CB 34	0	0	0.33 ± 0.03	0.46 ± 0.03	0.68 ± 0.03	1.30 ± 0.08
CB 54	0	0	1.07 ± 0.07	2.46 ± 0.04	19.71 ± 0.02	2.15 ± 0.04
CB 205.....	0	0	<0.14	...	...	...
CB 230.....	0	0	0.24 ± 0.05	0.17 ± 0.01	2.79 ± 0.04	0.64 ± 0.08
CB 232.....	0	12	<0.19	...	...	...
CB 244.....	0	0	0.38 ± 0.08	0.67 ± 0.06	4.31 ± 0.06	1.65 ± 0.16
CB 246.....	-20	-40	<0.25	...	...	...

NOTE.—Line parameters are derived from Gaussian fits (see § 3.1.2).
[a] Red and blue wings.

TABLE 10

LINE PARAMETERS OF THE IRAM $C^{34}S$ OBSERVATIONS

	OFFSETS		$C^{34}S$ $J = 2 \rightarrow 1$				$C^{34}S$ $J = 3 \rightarrow 2$			
SOURCE	$\Delta\alpha$ (arcsec)	$\Delta\delta$ (arcsec)	T_{mb} (K)	$\int T_{mb}\, dv$ (K km s^{-1})	V_{LSR} (km s^{-1})	ΔV (km s^{-1})	T_{mb} (K)	$\int T_{mb}\, dv$ (K km s^{-1})	V_{LSR} (km s^{-1})	ΔV (km s^{-1})
CB 6	0	0	<0.28	...	...	...	<0.21	...	...	...
CB 17	0	0	0.42 ± 0.09	0.17	-4.6	0.38	0.23 ± 0.06	0.08	-4.6	0.28
CB 54	0	0	0.46 ± 0.15	0.42	19.8	0.87	0.97 ± 0.28	0.68	19.8	0.66
CB 232.....	0	12	<0.46	...	...	...	<0.28	...	...	...
CB 243.....	0	12	<0.28	...	...	...	<0.18	...	...	...
CB 244.....	-12	0	0.35 ± 0.08	0.26	4.1	0.67	0.17 ± 0.06	0.14	4.1	0.74
CB 246.....	-20	-40	0.40 ± 0.12	0.12	-0.7	0.26	0.26 ± 0.06	0.09	-0.7	0.34

NOTE.—Line parameters are derived from Gaussian fits (see § 3.1.2).

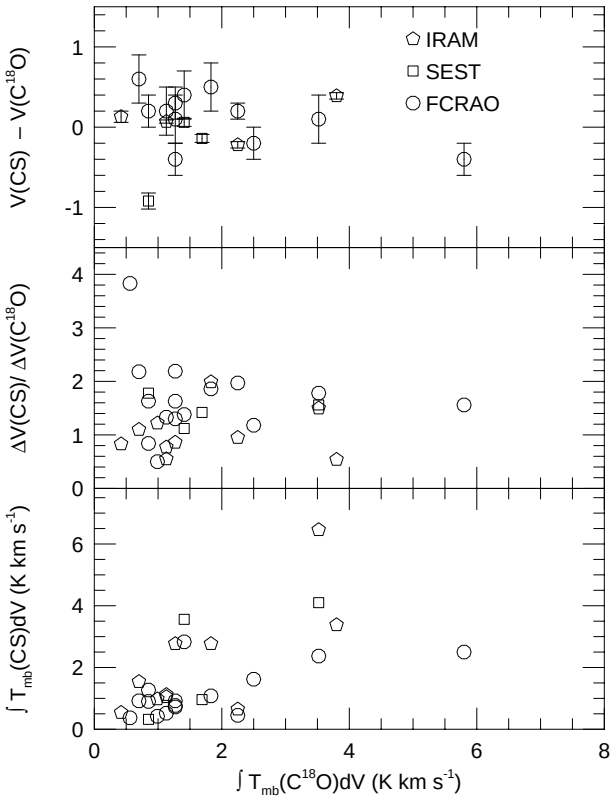

FIG. 3.—Integrated intensity of the CS $J = 2 \rightarrow 1$ lines are plotted vs. the same quantity for the $C^{18}O$ $J = 2 \rightarrow 1$ lines (Wang et al. 1995) in the bottom panel. In the middle panel, the ratio of CS line width to the $C^{18}O$ line width is plotted. In the top panel, the velocity difference between CS and $C^{18}O$ is plotted, with error bars calculated from the individual uncertainties, added in quadrature. For the SEST and IRAM data, the error bars reflect just the statistical uncertainties in the velocity from the Gaussian fit, probably unrealistically low. In all three panels, different symbols are used to plot the data from different telescopes, with the key given in the top panel. Statistics are given in the text.

sources also observed at SEST or IRAM, the line widths from FCRAO data were always larger, by a factor of 1.7 on average. The mean ratio of line widths, $\Delta V(\mathrm{CS})/\Delta V(\mathrm{C^{18}O})$, is 1.68 ± 0.75 for the FCRAO data, 1.47 ± 0.28 for the SEST data, and 1.03 ± 0.45 for the IRAM data. Since the IRAM data were obtained with a beam that is most similar to the 30″ beam of the $C^{18}O$ observations, these data suggest that the line widths of CS and $C^{18}O$ are similar when observed with similar spatial resolution. On an individual basis, the ratio of line widths varies from 0.5 to 2.0, indicative of real variations. The average CS $J = 2 \rightarrow 1$ line width of the IRAM spectra is 0.8 ± 0.4 km s^{-1}, with the most extreme values being 0.20 km s^{-1} (CB 184, Class II) and 2.0 km s^{-1} (CB 54, Class I, embedded cluster).

A comparison between the line velocities is consistent with the idea that the CS and $C^{18}O$ lines arise in similar regions. The top panel in Figure 3 shows the difference in velocity, with uncertainties. The error bars are statistical only for the SEST and IRAM data and are probably unrealistically low. For the FCRAO data, the differences are on average consistent with the uncertainties; $\langle V(\mathrm{CS}) - V(\mathrm{C^{18}O})/\sigma_{\delta V} \rangle = 1.2 \pm 0.7$, where $\sigma_{\delta V}$ is the uncertainty in the velocity difference, based on the uncertainties in the two velocities. The largest and most significant discrepancy is for CB 52, which has an uncertain fit and a self-absorbed line (see Table 5).

We compared the CS maps with the $C^{18}O$ maps, obtained with a 30″ beam by WEZC95, in nine sources that were mapped beyond their half-maximum intensities in both transitions. The $C^{18}O$ maps covered areas of $\lesssim 2'$, while the CS maps covered an area of $4' \times 5'$. Despite the different coverages and angular resolutions, the peaks and general morphologies of both maps agree in all nine sources, which again suggests that both lines trace the same gas. Minor differences are found in a number of sources. In CB 3, the CS map shows an additional clump to the north of the *IRAS* source, in a region not covered by the $C^{18}O$ map; in CB 68, the $C^{18}O$ map showed a well-defined peak around the *IRAS* source while the CS map reveals only diffuse, weak emission with an extension to the northwest. General agreement between the $C^{18}O$ maps and the CS maps suggests that the column density peaks in these globules indicated by the peaks in the $C^{18}O$ maps are likely to be the locations of dense gas, as indicated by the peaks of maps in density-sensitive CS emission.

The critical density ($n_c = A/\gamma$) of the CS $J = 2 \rightarrow 1$ line is 3.0×10^5 cm^{-3}, compared to 2.1×10^4 cm^{-3} for the $C^{18}O$ $J = 2 \rightarrow 1$ line. Accounting for trapping in CS with a typical $\tau = 4$ would lower the effective n_c to about 8×10^4 cm^{-3}. The critical density is not a reliable guide to the actual density, but the difference between CS and $C^{18}O$ indicates that CS should be reflective of denser gas than is $C^{18}O$. In fact, the similarity between the two lines in the detection rates, the correlation of integrated intensities, and the similarities of the mean line width, center velocity, and map morphology all suggest that, on average, a high column density in a globule indicates the presence of a dense core.

The maps of CB 34 and CB 54 agree well with maps of those cores in HCN (Afonso et al. 1998), but the HCN map of CB 68 shows a clear peak at our (0,0) position instead of the diffuse, weak emission seen in the CS $J = 2 \rightarrow 1$ line.

Launhardt & Henning (1997) have also found a good correlation between the peak temperature of CS $J = 2 \rightarrow 1$ and the 1.3 mm continuum emission (see their Fig. 10), even though CS is generally opaque and the 1.3 mm continuum emission is optically thin. The correlation is less clear but still present when using the integrated CS line intensities instead of the peak temperatures. This correlation and the one in Figure 3 suggest that the strength of an optically thick, but unthermalized, line will continue to grow with column density because of trapping. Hogerheijde et al. (1997) found a similar result for HCO^+ lines, if the $J = 1 \rightarrow 0$ line is excepted.

We compared the CS maps with the 1.3 mm dust continuum maps, obtained with a 11″ beam by Launhardt et al. (1998b), in eight sources that were mapped in both tracers. In six of these globules (CB 3, 34, 54, 230, 232, and 244), the dust continuum peaks agree well with the CS peaks, which suggests that both tracers are sensitive to the dense cores and that CS cannot be completely frozen out from the gas phase. However, in two other globules (CB 68 and 243), strong dust continuum emission peaks were found at the position of the *IRAS* sources, while no CS emission peak was found at these positions in the FCRAO maps. In CB 243, there was, however, relatively strong CS emission found at the *IRAS* position in the smaller IRAM beam. Both sources are candidate Class 0 sources. In such cold and dense cores, both optical depth effects and depletion of CS onto grains can affect the CS emission. These sources will be discussed in more detail by Launhardt et al. (1998b).

4.2. *Sizes and Masses*

For the nine sources with adequate CS maps (CB 3, 12, 34, 44, 54, 216, 230, 232, and 244), angular sizes along major and minor axes of the half-maximum contour were extracted. Assuming a Gaussian shape for both source and beam, each angular size was corrected for beam broadening to obtain corrected sizes along the major and minor axes ($\theta_{\rm max}$ and $\theta_{\rm min}$, respectively). The ellipticity (e) was calculated from $\theta_{\rm max}/\theta_{\rm min}$. These values are given in Table 11. We also give the distance estimate from LH97 and the reliability class assigned by them, where available. Reliability class A implies an accuracy of about 30%, while class B implies considerable uncertainty. Using the distance, a linear size (l) was calculated from the geometric mean of the major and minor axis sizes. The average size of the CS cores is 0.41 ± 0.18 pc. Excluding the three most massive sources that are either associated with embedded clusters (CB 34 and 54, Alves & Yun 1995, and Launhardt et al. 1998b) or with a distant high-mass star-forming region (CB 3, Launhardt, Henning, & Klein 1998a), the average size of the CS cores of "typical" globules amounts to 0.33 ± 0.15 pc.

Finally, using the line width (ΔV) from Table 4 and the distance, a virial mass was computed from

$$M_V = \frac{5}{3}\frac{l v_{\rm rms}^2}{2G},$$

where $v_{\rm rms} = 3^{1/2}\,\Delta V/2.35$. The line widths of the CS lines are certainly overestimated in some cases (see § 4.1). Consequently, we give the virial masses computed from the CS size but with the $C^{18}O$ line width in Table 11, along with virial masses computed from the same method applied to the $C^{18}O$ maps in WEZC95. These masses differ from those in WEZC95 largely because we use the distances of LH97 instead of one average distance of 600 pc but also because of some other corrections. The average virial mass calculated from the CS maps is $M_V({\rm CS}) = 60 \pm 52\ M_\odot$. Excluding again the three most massive cores, the average virial mass of the "typical" globule cores amounts to $M_V({\rm CS}) = 26 \pm 12\ M_\odot$. The virial masses calculated from the CS maps (except CB 3) are on average 3 ± 1.3 times larger than the masses calculated from the $C^{18}O$ maps. Since we are using the line widths from $C^{18}O$ in both cases, the difference in masses reflects the larger size of the cores in the CS $J = 2 \rightarrow 1$ line compared to the $C^{18}O$ $J = 2 \rightarrow 1$ line (average size of 0.21 ± 0.24 pc). The larger size of the CS cores is interesting in view of the higher critical density of CS; it probably reflects the higher optical depth of CS and the lower spatial resolution of the CS maps.

We can compare the sizes measured for these globules with those measured for other kinds of objects. The Taurus cores mapped by Zhou et al. (1994b) in $C^{18}O$ $J = 2 \rightarrow 1$ have an average size of $l = 0.094 \pm 0.05$ pc, about half the average of the sizes of this sample measured with the $C^{18}O$ $J = 2 \rightarrow 1$ line. A study of cores selected to have H_2O masers and measured in the $J = 2 \rightarrow 1$ line of $C^{34}S$ (Juvela 1996) had an average size of 1.22 ± 0.51 pc, more than 3 times the mean value for our sample. A similar sample of cores in the northern hemisphere, measured in the $J = 5 \rightarrow 4$ line of CS has an average size of 1.0 pc (Plume et al. 1997), although a follow-up study of more sources has yielded a mean size of 0.70 pc (Y. Shirley, private communication). The Bok globules that were mapped have sizes intermediate between cores in the nearby Taurus cloud that are forming low-mass stars and more distant cores that are forming more massive stars. To some extent, the differences result from selection effects because only large sources can be detected and mapped at large distances. The nearby globules are more similar to the Taurus cores in size.

4.3. *Evolutionary Connections*

The complete detection of the Class 0 and I sources versus the lower detection rates for the other groups of globules reflects the fact that these young objects are always deeply embedded in dense molecular cloud cores. The fact that all four Class 0 candidates have strong CS emission confirms that these sources are the most deeply embedded sources of our sample.

In contrast, the more evolved Class II-D and II sources are, in general, embedded in less massive and less dense cloud cores. They may have partially destroyed their parental molecular cloud cores or moved away from them. LH97 have shown that the *IRAS* point sources associated with these globules (their group 3 corresponds roughly to Class II) usually lie outside the opaque parts of the globule. Large-scale CS mapping which covers the *IRAS* Point Source Catalog (hereafter IPSC) position as well as the opaque center of the globule is needed to clarify this question.

The lower detection rate for the "starless" globules compared to the globules with *IRAS* point sources, especially those of Class 0 and I, suggests that dense cores are less common in these globules. But the absence of an IPSC reference position means that some of the nondetected

TABLE 11

SIZE AND MASS

SOURCE	SIZES $\theta_{\rm max}$ (arcsec)	SIZES $\theta_{\rm min}$ (arcsec)	e	DISTANCE (pc)	RELIABILITY	l (pc)	M_V(CS) ($M_\odot$)	M_V($C^{18}O$) ($M_\odot$)
CB 3	41	24	1.7	2500	B	0.38	99	196
CB 12	216	54	4.0	800	B	0.42	35	10
CB 34	133	75	1.8	1500	A	0.73	170	...
CB 44	107	58	1.8	1500[a]	B	0.57	37	...
CB 54	116	54	2.1	1500	B	0.58	116	31
CB 216.....	112	24	4.7	700	A	0.18	22	15
CB 230.....	126	54	2.3	450	A	0.18	12	8
CB 232.....	186	107	1.7	600	B	0.41	42	16
CB 244[b].....	270	215	1.3	180	B	0.21	10	2

[a] This paper; derived with the same method as described in LH97.

[b] The half-power contour was extrapolated to close it; size will be underestimated.

globules might have dense cores at different positions. Therefore, our detection rate might underestimate the frequency of dense cores within this group of globules.

Comparison of the average line intensities and line widths of different globule groups when measured with the same telescope reveals that the CS line characteristics change with the expected evolutionary stage of the embedded objects. At all three telescopes, the average line intensities are larger for globules with *IRAS* point sources than for "starless" globules: FCRAO: 1.1 ± 0.8 versus 0.5 ± 0.5 K km s^{-1}; SEST: 1.7 ± 1.7 versus 0.7 K km s^{-1} (only one starless globule); and IRAM: 1.7 ± 1.7 versus 1.0 K km s^{-1} (only one starless globule). Furthermore, the integrated line intensities of the Class 0 and I sources are larger than the average values for all other globules with *IRAS* point sources: FCRAO: 1.3 ± 0.9 versus 0.8 ± 0.4 K km s^{-1}, SEST: 2.9 ± 1.3 versus 0.5 ± 0.3 K km s^{-1}, and IRAM: 1.8 ± 1.5 versus 0.2 K km s^{-1} (only one Class II source detected). This trend was also seen in HCN (Afonso et al. 1998). These trends suggest that the cores of globules with embedded Class 0 and I sources have, on average, higher densities than the cores of "starless" globules and of globules with embedded Class II sources. Detection of the CS $J = 5 \rightarrow 4$ emission toward seven of 10 sources with the strongest CS $J = 2 \rightarrow 1$ emission supports the presence of higher density gas. Six of these are Class I sources, and one source is a candidate Class 0 source (CB 17). Three sources, CB 3, CB 54, and CB 244, estimated to have densities of 2×10^5 to 2×10^6 cm^{-3} from the C^{18}O and H_2CO lines (WEZC95), have the strongest CS $J = 5 \rightarrow 4$ intensities.

The same trend can be seen in the observed line widths. At all three telescopes, the average line widths of globules with *IRAS* point sources are larger than for "starless" globules: FCRAO: 1.8 ± 0.5 versus 1.5 ± 0.1 km s^{-1}; SEST: 1.5 ± 0.5 versus 0.6 km s^{-1} (only one starless globule); and IRAM: 0.86 ± 0.43 versus 0.52 km s^{-1} (only one starless globule). Furthermore, the line widths of the Class 0 and I sources are slightly larger than the average values for all other globules with *IRAS* point sources: FCRAO: 1.9 ± 0.6 versus 1.6 ± 0.4 km s^{-1}; SEST: 1.7 ± 0.3 versus 1.2 ± 0.3 km s^{-1}; and IRAM: 0.9 ± 0.4 versus 0.2 km s^{-1} (only one Class II source detected). This line broadening may indicate higher optical depths (i.e., more dense gas and higher densities) as well as a more complex gas dynamics (e.g., turbulence, outflows, infall, rotation) in globules with embedded Class 0 and I sources compared to "starless" globules and globules with embedded Class II sources.

Self-absorption dips in the optically thick CS lines are indicative of a radial gradient in the excitation conditions (density, temperature). A blue asymmetry, as seen in five globules (CB 17, 54, 214, 224, and 230) is consistent with mass infall (see, e.g., Zhou & Evans 1994). Although complete maps of optically thick lines tracing different density regimes are necessary to prove the infall hypothesis, these globules are good collapse candidates. CB 54 and CB 244 were already classified by WEZC95 as collapse candidates. In CB 244, the CS $J = 2 \rightarrow 1$ line has a red asymmetry, while the CS $J = 3 \rightarrow 2$ line has a blue asymmetry.

Line wings in the CS emission, as seen in six globules (CB 3, 6, 34, 205, 232, 244), are indicative of high densities in the outflowing gas. The only globule with CS line wings in which no CO outflow had been detected yet (CB 6) has a cometary-shaped near-infrared nebula associated with the *IRAS* point source. This nebula very likely represents the unobscured part of a bipolar nebula (Yun & Clemens 1994; Launhardt 1996); the CS line wing makes this source another outflow candidate among the CB globules.

5. SUMMARY

A sample of 47 Bok globules was surveyed for CS emission, and 32 globules (68%) were detected in the CS $J = 2 \rightarrow 1$ line. The detection rate for globules with *IRAS* sources is higher (72%) than for those without *IRAS* sources (44%), especially for the stronger lines. The highest detection rate was found for globules with embedded Class 0 and Class I infrared sources (100%). Among the outflow sources, the detection rate was also very high (79%). Higher rotational lines were detected for a substantial fraction (68% for the $J = 3 \rightarrow 2$ line and 57% for the $J = 5 \rightarrow 4$ line) of the subsample in which they were searched. Lines of C^{34}S were detected in 57% of a small subsample and indicated typical optical depths of 3–5 for the $J = 2 \rightarrow 1$ line of CS.

CS $J = 2 \rightarrow 1$ maps of 12 sources were presented; the maps generally agreed well with maps of C^{18}O and HCN, and the peaks usually agreed with the locations of the *IRAS* sources. The sources with good agreement also tend to have prominent cores in the C^{18}O maps, to have CO outflows and H_2CO emission, and to have infrared/millimeter sources with Class 0 and I SEDs.

The similarity of detection statistics, line width, and map morphology between the CS $J = 2 \rightarrow 1$ line and the C^{18}O $J = 2 \rightarrow 1$ line, along with the correlation of integrated intensities of these two lines, suggests that column density peaks (traced by C^{18}O) generally correspond to locations of relatively dense gas (traced by the CS).

We determined sizes for the sources with suitable maps and compared the results to studies of regions selected in different ways. The globules studied here cover a broad range of sizes and masses, overlapping dense cores in nearby regions on the low end and more distant regions with embedded clusters of YSOs on the high end. The mean size and virial mass of the CS cores studied here are 0.4 ± 0.2 pc and $60 \pm 52\ M_\odot$. The mean size and virial mass of the CS cores of typical nearby globules (excluding the three most massive sources with embedded clusters) are 0.33 ± 0.15 pc and $26 \pm 12\ M_\odot$.

We are grateful to the staffs of the four telescopes used in this research for their assistance. R. L. acknowledges support through the Verbundforschung Astronomie/Astrophysik grant 50 OR 9414 9. N. J. E. acknowledges support from NSF (AST 93-17567). D. C. acknowledges support from NSF (AST 92-21194) and NASA (NAG 5-1997 and 5-3337).

REFERENCES

Afonso, J. M., Yun, J. L., & Clemens, D. P. 1998, AJ, 115, 1111
Alves, J. F., & Yun, J. L. 1995, ApJ, 438, L107
André, P., Ward-Thompson, D., & Barsony, M. 1993, ApJ, 406, 122
Bok, B. J., & Reilly, E. F. 1947, ApJ, 105, 255
Bourke, T. L., Hyland, A. R., Robinson, G., James, S. D., & Wright, C. M. 1995, MNRAS, 276, 1067
Chandler, C. J., & Sargent, A. I. 1993, ApJ, 414, L29
Choi, M., Evans, N. J., II, Gregersen, E. M., & Wang, Y. 1995, ApJ, 448, 742
Clemens, D. P., & Barvainis, R. 1988, ApJS, 68, 257 (CB)
Clemens, D. P., Yun, J. L., & Heyer, M. H. 1991, ApJS, 75, 877
Erickson, N. R., Goldsmith, P. F., Novak, G., Grosslein, R. M., Viscuso, P. J., Erickson, R. B., & Predmore, C. R. 1992, IEEE MTT, 40, 1
Henning, Th., & Launhardt, R. 1998, A&A, in press
Hogerheijde, M. R., van Dishoeck, E. F., Blake, G. A., & van Langevelde, H. J. 1997, ApJ, 489, 293
Juvela, M. 1996, A&AS, 118, 191
Kane, B. D., Clemens, D. P., & Myers, P. C. 1994, ApJ, 433, L49
Kutner, M. L., & Ulich, B. L. 1981, ApJ, 250, 341
Lada, C. J. 1987, in Star Forming Regions, ed. M. Peimbert & J. Jugaku (Dordrecht: Reidel), 1
Launhardt, R. 1996, Ph.D. thesis, Univ. of Jena
Launhardt, R., & Henning, Th. 1997, A&A, 326, 329 (LH97)
Launhardt, R., Henning, Th., & Klein, R. 1998a, in ASP Conf. Proc. 132, Star Formation with the Infrared Space Observatory, ed. J. L. Yun & R. Liseau (San Francisco: ASP), 119
Launhardt, R., Ward-Thompson, D., & Henning, Th. 1997, MNRAS, 288, L45
Launhardt, R., Zylka, R., & Henning, Th. 1998b, in preparation
Lemme, C., Wilson, T. L., Tieftrunk, A. R., & Henkel, C. 1996, A&A, 312, 585
Leung, C. M., Kutner, M. L., & Mead, K. N. 1982, ApJ, 262, 583
Mangum, J. 1993, PASP, 105, 117
Martin, R. N., & Barrett, A. H. 1978, ApJS, 36, 1
Mauersberger, R., Guélin, M., Martín-Pintado, J., Thum, C. Cernicharo, J., Hein, H., & Navarro, S. 1989, A&AS, 79, 217
Moreira, M. C., Yun, J. L., Torrelles, J. M., & Vazquez, R. 1997, AJ, 113, 1371
Neckel, T., & Staude, H. J. 1990, A&A, 231, 165
Penzias, A., & Burrus, C. 1973, ARA&A, 11, 51
Plume, R., Jaffe, D. T., Evans, N. J., II, Martín-Pintado, J., & Gómez-González, J. 1997, ApJ, 476, 730
Turner, B. E. 1993, ApJ, 411, 219
———. 1994a, ApJ, 420, 661
———. 1994b, ApJ, 437, 658
Velusamy, T., Kuiper, T. B. H., & Langer, W. D. 1995, ApJ, 451, L75
Villere, K. R., & Black, D. C. 1982, ApJ, 252, 524
Wang, Y., Evans, N. J., II, Zhou, S., & Clemens, D. P. 1995, ApJ, 454, 217 (WEZC95)
Wilking, B. A., Lada, C. J., & Young, E. T. 1989, ApJ, 340, 823
Yun, J. L. 1993, Ph.D. thesis, Boston Univ.
Yun, J. L., & Clemens, D. P. 1990, ApJ, 365, L73 (YC90)
———. 1992, ApJ, 385, L21 (YC92)
———. 1994, AJ, 108, 612
———. 1995, AJ, 109, 742
Zhou, S., & Evans, N. J., II. 1994, in ASP Conf. Proc. 65, Clouds, Cores, and Low Mass Stars, ed. D. P. Clemens & R. Barvainis (San Fransisco: ASP), 183
Zhou, S., Evans, N. J., II, Kömpe, C., & Walmsley, C. M. 1993, ApJ, 404, 232
———. 1994a, ApJ, 421, 854
Zhou, S., Evans, N. J., II, Wang, Y., Peng, R., & Lo, K. Y. 1994b, ApJ, 433, 131